Title: The effects of fiber diameter and spacing-size of an artificial scaffold on the *in vivo* cellular response and tissue remodeling

Tsunehito Horii[*1,2], Hiroyuki Tsujimoto[1,2], Akeo Hagiwara[1,2], Noritaka Isogai[3], Yu Sueyoshi[3], Yasumitsu Oe[4], Susumu Kageyama[1], Tetsuya Yoshida[1], Kenichi Kobayashi[1], Hiroshi Minato[5], Joe Ueda[6], Hiroshi Ichikawa[2], Akihiro Kawauchi[1]

[1]Department of Urology, Shiga University of medical science, Seta Tsukinowa, Otsu, Shiga, 610-0321, Japan

[2]Division of Medical Life System, Department of Life and Medical Science, Doshisha University, Kyotanabe, Kyoto 610-0394, Japan

[3]Department of Plastic and Reconstructive Surgery, Kindai University, Osaka 589-0014, Japan

[4]Department of Gastroenterology, Kusatsu General Hospital, Yabase, Kusatsu, Shiga 525-8585, Japan

[5]Department of Surgery, Yawata Chuo Hospital, Yawatagotanda, Yawata, Kyoto 614-8071, Japan

[6]Department of Gastroenterology, Ueda Clinic, Kitanakaieshita, Takanosu, Akita 018-3331, Japan

Author for correspondence: Tsunehito Horii

Department of Urology, Shiga University of medical science, Seta Tsukinowa, Otsu, Shiga, 610-0321, Japan

Tel: +81-77-548-2273 Fax: +81-77-548-2400

E-mail: thorii@belle.shiga-med.ac.jp

Abstract:

By mimicking the extracellular matrix, non-woven fabrics can function as scaffolds for tissue engineering application ideally, and they have been characterized regarding their fiber diameter and fiber spacing (spacing-size) *in vitro*. We chronologically examined the *in vivo* effects of these fabrics on the cellular response and tissue remodeling. Four types of non-woven poly-glycolic acid (PGA) fabrics (Fabric-0.7, Fabric-0.9, Fabric-3, Fabric-16 with fiber diameters of 0.7, 0.9, 3.0 and 16.2 μm, and spacing-sizes of 2.0, 19.3, 19.0 and 825.4 μm, respectively) were implanted into the rat dorsum, and subjected to histologic and immunohistochemical analyses from days 3 to 70. With Fabric-0.7, inflammatory cells (mainly M1 macrophages), and myofibroblasts with collagen type III accumulated mainly on the surface of the fabric and did not infiltrate inside the fabric initially, likely due to the narrow fiber space. Massive formation of collagen type I then appeared with the degradation of the fabrics, and finally, the remodeled tissue turned into dense scar. With Fabric-0.9 and Fabric-3, inflammatory cells (predominantly M2 macrophages), were seen in all layers of the fabric initially. A mild increase in collagen type I was then seen, with few myofibroblasts, and the remodeled tissue ultimately showed relatively little scar with adequate thickness of the tissue induced by the fabrics. With Fabric-16, inflammatory cells (predominantly M1 macrophages), infiltrated into all layers of the fabric initially along with many myofibroblasts especially in the hole. Lately, massive formation of collagen type I was noted due to the slow degradation of the fabric, with the shrank of the fabric substantially and the remodeled tissue finally turned to dense scar. These findings suggest that optimizing the spacing-size as well as the fiber diameter of artificial scaffolds may control the cellular response and tissue remodeling and facilitate favorable tissue regeneration without scar formation.

Key words: Nonwoven fabric, Tissue engineering, Cellular response, M1/M2 macrophages, Tissue remodeling

INTRODUCTION

Wound repair is one of the most complex biological processes, especially in mammals and human beings[1]. After an injury, multiple biological pathways are immediately activated and synchronized to achieve the injured tissue regeneration. However, the wound repair process often leads to a non-functioning fibrotic tissue mass known as a scar. To manipulate more regenerative wound repair without scar formation, various artificial regenerative methods have been developed. Among those methods, artificial scaffolds have been used extensively in experimental and clinical settings[2-4].

Ideally, the artificial scaffolds should promote the process of the cellular adhesion, proliferation and differentiation. Non-woven fabrics have been widely used as effective artificial scaffolds in the field of regenerative medicine[5-8]. These non-woven fabrics are made from various materials including natural ones (e.g. collagen, gelatin, alginate) or synthetic ones (e.g. poly-glycolic acid [PGA], poly-lactic acid [PLA]). While the properties of non-woven fabrics generally depend on the composition material, the fabrics are also characterized in terms of the size of fiber diameter and fiber spacing (spacing-size), especially for fabrics made using the same materials[9]. Several *in vitro* studies have reported that the fiber diameter and spacing-size affect not only the cellar adhesion and proliferation, but also the related cell differentiation, such as the macrophage phenotype[5,6,8,10]. However, few *in vivo* studies have investigated the effects of fiber diameter and spacing-size on the cellular response and tissue remodeling after the implantation of artificial scaffolds[11,12].

In this study, we implanted four types of synthetic PGA fabrics with different fiber diameters and spacing-size as artificial scaffolds into the back of rats (rat dorsal implantation model). Then, we chronologically examined the differences in the *in vivo* effects on the cellular response and tissue remodeling such as the population of inflammatory cells, amount of granulation tissues and accumulation of connective tissues on the individual PGA fabrics. In addition, we revealed the unique features, such as the transition of collagen subtypes (from type III to type I), myofibroblast and vascular endothelial cell migration, and the phenotypic or functional polarization of macrophages (M1 [inflammatory macrophages] or M2 [regenerative macrophages]), depending on

the differences of the fiber diameter and spacing-size.

MATERIALS AND METHODS

1. Preparation of non-woven PGA fabrics

In this study, we used four types of PGA non-woven fabrics with different fiber diameters and spacing sizes (Fabric-0.7, Fabric-0.9, Fabric-3 and Fabric-16) as shown in Figure 1. Fabric-0.7 was created using the electrospinning method, as described previously[13,14]. In brief, PGA polymer powder (BMG Co., Kyoto Japan) was dissolved in 1,1,1,3,3,3 hexafluoro-2-propanol (HFIP, Sigma-Aldrich Co., Missouri, USA) at the concentration of 15%. The PGA polymer solution was then placed in a 10 ml syringe fitted with a 23 G needle (Terumo Co., Tokyo, Japan). Voltage was applied using a high-voltage power supply (9.0kV) at a distance of approximately 5 cm between the grounded target (cathode) and the needle tip (anode). The polymer solution was drawn from the syringe, forming a pendant drop at the tip of the needle by combining the force of gravity and an electrostatic charge. A positively charged jet ejected from the drop was splayed onto the negatively charged target. The rotation of the target was 300 rpm and the traverse speed was 31 cm/min. A non-woven fabric structure was then formed on the collecting tube.

Fabric-0.9 and Fabric-3 were created using the melt-blowing method with a single screw meltblown apparatus (Nippon Nozzle, Kobe, Japan), as described previously[14]. In Brief, the PGA polymers solution described above were fed into hopper and moved into the extruder, which has six adjustable heating zones. The melted PGA polymer with adequate viscosity was then moved to a spinning pump and extruded through die holes. The droplets changed to the short fibers by high velocity hot and dry air streams after extrusion. The fibers were collected on the surface of a rotating drum with an air suction equipment. The solid fibers were finally wound up by winding frame. In the meltblown method, we used following parameters; the range of temperatures of extrusion zones were 180 °C to 200 °C and the air temperature was 220 °C. The die collecter distance was 25 cm and the speed was 0.5 rpm.

Fabric-16 was purchased from GUNZE Ltd., (Neoveil®, Kyoto, Japan). The PGA polymers

formed piled fibers, and the fibers were formed into extended sheets of short fiber webs. The sheets of fibers was then stabbed with of needle-punch barbs to entangle them.

Ethylene-oxide gas (EOG) sterilization was performed at the Central Research Laboratory Shiga University of Medical Science, applying a low-temperature cycle (37 °C). Before sterilization, the samples were placed in an appropriate package with a specific indicator that proved the suitability of the EOG concentration and the duration. The samples were then sterilized by EOG sterilization apparatus (FRH16, Iki Co., Otsu, Japan) (0.43 g/L at 40 °C for 4 h).[15] After EOG sterilization, the residual gas in the fabrics were removed by a blast drying oven (AVO-250N; As One, Osaka, Japan) at 37 °C for 48 h. The fabrics were then stored in a desiccator until used for experiments.

2. Fiber diameter and spacing-size of non-woven PGA fabrics

For the four types of PGA fabrics, the fiber diameters and spacing-size of each fabric were measured using the scanning electron microscopy (SEM). The average fiber diameter was calculated using Image J software program (ImageJ, U.S. National Institutes of Health, Maryland, USA) with 30 randomly selected fibers appearing in the top layer of the SEM micrograph. The value was presented as the mean ± standard deviation (SD).

Next, the distance between fiber-edges and the neighboring fiber-edges was defined as the fiber spacing-size. The spacing-sizes of Fabric-0.7, 0.9 and 3 were measured using SEM images of the cross-section surface after being frozen in liquid nitrogen. Thirty different spacing-sizes were randomly selected and evaluated using the Image J software program. Finally, the average spacing-sizes was calculated and presented as the mean ± SD.

The spacing-size of Fabric-16 was also measured using the cross-section surface of SEM images after being frozen in liquid nitrogen with the Image J software program. However, Fabric-16 has a complex appearance composed of two kinds of structures with different spacing-sizes due to its needle-punch production process. One of the two structures is "the fiber bundle" and the other is the "hole" surrounded by the bundles. To measure the spacing-sizes of the “fiber bundle” and “hole”,

30 different spacing-sizes were randomly selected and measured using SEM images. Each average spacing-size was then calculated and presented as the mean ± SD.

3. *In vivo* rat dorsal subcutaneous implantation

A total of 36 female Wistar/ST rats (7 weeks of age, weighing approximately 200-220 g) were purchased from Shimizu Animal Laboratory (Kyoto, Japan) a week before the examination. The rats were kept in a specific-pathogen-free condition room with a 12 h light-dark cycle, mean temperature of 23°C and mean humidity of 50%. Standard laboratory rodent chow and water were freely available. All animal experiments, animal care, housing and surgical procedures complied with the instructional guidelines of the Committee for Animal Research of Shiga University of Medical Science and Doshisha University.

Each rat was given ethyl ether (Diethyl Ether®; Wako, Inc., Osaka, Japan) for inhalation anesthesia. Sodium pentobarbital (5 mg, Somnopentyl®; Kyoritsu Seiyaku, Inc., Tokyo, Japan) was diluted into 1 ml saline solution, and then the sodium pentobarbital was administered intraperitoneally to each rat with a tuberculin syringe and 23 G injection needles. Four 1.5 cm lateral incisions were made on the dorsal skin of each rat and each incision was fashioned into a 1.5×1.5 cm “pocket” in the subcutaneous layer. Each of the four different PGA non-woven fabrics was cut into a square-shaped sheet measuring 10×10 mm in size and 3.8 mg in weight. A piece of the square sheet of each type of fabrics was placed into the one of the four pockets on each rat in a randomized manner. Six rats were sacrificed after each time point: 3, 7, 14, 21, 35 and 70 days.

4. Histologic and immunohistochemical analyses

The implanted PGA non-woven fabrics and surrounding tissues were surgically excised *en bloc* as these specimens for microscopic examinations. These specimens were fixed with 10% formaldehyde and processed for embedding in paraffin. The embedded samples were sectioned at 3 μm thickness and stained with hematoxylin and eosin staining (H&E staining) or Masson trichrome staining. We carefully observed all samples, paying close attention to histological factors, such as

inflammatory cell infiltration, granulation tissue formation and connective tissue formation by H&E staining and Masson trichrome staining at first. We then quantitatively classified the status of the above histological factors using a zero-to-three grading scale for the scoring, in comparison with adjacent normal parts, as shown in Table I. Especially, for Fabric-16, we evaluated the histologic findings separately for each of the two portions of the structure with different spacing-sizes: the "fiber bundle" (Fabric-16 FB) and "hole" (Fabric-16 HL).

Using all specimens stained with H&E staining, the thickness of each PGA fabric itself as well as the tissues induced by the implanted fabrics, which included the inflammatory cells, granulation tissues and connective tissues, were measured, respectively. The thicknesses of the fabrics and tissues were measured in six microscope fields at 400× magnification for each specimen and averaged at each time point.

In addition, to investigate the process underlying the tissue remodeling induced by each PGA fabric, we paid special attention for the i) presence of myofibroblasts (stained by α-SMA), ii) intensity or transition of collagen type I and III production, iii) presence of migrated vessels (stained by Von Willebrand Factor) and iv) phenotype of the migrated macrophages (M1 or M2). In detail, the specimens were immunostained for α-smooth muscle actin (α-SMA; Agilent Technologies Japan, Ltd., Tokyo, Japan), collagen type I (Anti-Collagen Type I; Acris OriGene Co., Rockville, MD, USA), collagen type III (Anti-Collagen Type III; Acris OriGene Co.), Von Willebrand Factor (VWF; abcam plc., Cambridge, UK), CD68 (Anti-CD68; abcam plc.) and CD163 (Anti-CD163; Abcam plc.) and observed carefully. We then quantitatively classified the status of the above factors i)-iv) using a zero-to-three grading scale for the scoring in 6 microscope fields at 400× magnification for each specimen in comparison with the adjacent normal parts, as shown in Table II. The scores at each time point were described as the average ± SD.

Statistical comparisons were performed using Steel-Dwass' test following the Kruskal-Wallis test. A p value of less than 0.05 was considered to be significant.

RESULTS

1. Fiber diameter and spacing-size of non-woven PGA fabrics

The fiber diameter and spacing-size of each PGA non-woven fabric is summarized in Table III. The SEM micrographs of the top layer and cross-section surface are shown in Figure 1. The fiber diameters of Fabric-0.7, 0.9, 3 were 0.69 ± 0.28, 0.9 ± 0.65 and 3.0 ± 1.86 μm, respectively. The spacing-size of Fabric-0.7, 0.9, 3 were 2.0 ± 0.8, 19.3 ± 7.8 and 19.0 ± 10.0 μm, respectively. The fiber diameter of Fabric-16 was 16.2 ± 1.1 μm. However, as described in the Materials and Methods, Fabric-16 has a structure composed of two kinds of locations with different two spacing-sizes ("fiber bundle" and "hole"). The spacing-size of the fiber bundle was 5.0 ± 4.0 μm, and that of the hole was 825.4 ± 126.9 μm.

2. Histologic and immunohistochemical analyses

2-1. Hematoxylin-eosin staining and Masson trichrome staining

The microscopic views and the scores with H&E staining and Masson trichrome staining of the 4 kinds of PGA non-woven fabrics at day 3, 7, 14, 35, and 70 are shown in Figure 2, 3 and 4-I A, B, C, respectively. In Fabric-0.7, the inflammatory cells and granulation tissue were seen into the superficial layers of the fabrics at day 3 (the average scores ± SD; 0.83 ± 0.41 and 0.67 ± 0.41) and 7 (1.33 ± 0.52 and 1.08 ± 0.58). From day 14, these cells and tissue spread throughout all layers (2.17 ± 0.26 and 2.17 ± 0.26) and began to decrease until day 70 (0.83 ± 0.26 and 1.00 ± 0.00). Whereas, connective tissue was observed on the surface of the fabric at day 7 (0.67 ± 0.52) but also in the central layer at day 14 (1.33 ± 0.52), and massively at days 35 (2.33 ± 0.52) to 70 (2.17 ± 0.75). Fibers of Fabric-0.7 were seen until day 14 but were barely visible any longer from day 35. The thickness of each fabric and the tissue induced by each fabric are shown in Figure 4-II A, B. The thickness of the Fabric-0.7 or the tissues induced by Fabric-0.7 approximately three times as high as the initial thickness of the fabric at day 14, and then turned to decreased rapidly. The fabric disappeared with the degradation of the fabric at day 35, while the induced tissue finally got two times level at day 70.

With Fabric-0.9 and 3, the inflammatory cells and granulation tissue were seen at the-

superficial layers of the fabrics on day 3 (1.83 ± 0.52 and 1.17 ± 0.41, 1.75 ± 0.52 and 1.25 ± 0.27) and throughout all layers of the fabric at day 7 (2.25 ± 0.69 and 2.08 ± 0.66, 1.92 ± 0.58 and 1.67 ± 0.61). These cells and tissue increased maximally at day 7 and began to decrease until day 70 (0.83 ± 0.26 and 0.83 ± 0.52, 0.50 ± 0.32 and 0.50 ± 0.32). Whereas, connective tissue was observed throughout the fabrics from day 7 (0.83 ± 0.41, 1.00 ± 0.00) and then increased mildly up to day 35 (1.50 ± 0.55, 1.33 ± 0.32) and maintained through day 70 (1.17 ± 0.41, 1.33 ± 0.52). The thicknesses of the Fabric-0.9 and 3 as well as the tissues induced by those fabrics increased more rapidly than those of other fabrics from day 3 and peaked approximately four or five times as high as the initial thickness at day 14, respectively. The fabrics then began to decrease and disappeared by day 70. The thicknesses of the induced tissues also began to decrease at day 35 but were still maintained three times level at day 70.

With Fabric-16, inflammatory cells and granulation tissue were seen throughout all layers of the fabric, especially around the bundles (16 FB) at day 3 (1.75 ± 0.52 and 1.08 ± 0.20). These cells and tissue showed a massive increase at day 7 (2.33 ± 0.52 and 2.08 ± 0.38) and hardly decreased at all until day 70 (1.83 ± 0.26 and 1.83 ± 0.75). In contrast, in the holes (16 HL), they increased until day 7 (1.92 ± 0.38 and 1.75 ± 0.42) but decreased gradually from day 14 (1.50 ± 0.55 and 1.83 ± 0.41) to 70 (0.67 ± 0.52 and 1.00 ± 0.00). Connective tissue was observed, especially in the holes, at day 7 (1.33 ± 0.52) and increased markedly until day 35 (2.50 ± 0.55) and showed almost no decrease until day 70 (2.17 ± 0.41). Whereas the tissue around the bundles showed almost no increase up to day 70 (1.50 ± 0.55). The spacing-size of the "hole" decreased with time from day 14 and had narrowed markedly, with a dense connective tissue layer to day 70. The thickness of the Fabric-16 and the tissues induced by Fabric-16 increased gradually but peaked only two times as high as the initial thickness at day 14. Then, those thickness maintained 1.5 or 2 times levels without complete degradation of the fabric until day 70, respectively.

The scores of inflammatory cells and granulation tissue in Fabric-16 FB were significantly higher than those in Fabric-0.7 and 16 HL at day 35 and those of Fabric-0.7, 0.9, 3 and 16 HL at day 70 (p<0.05). The scores of connective tissue formation in Fabric-0.9, 3 and 16FB peaked at day 14

and were maintained until day 70, whereas those in Fabric-0.7 and 16 HL peaked at day 35 and remained high until day 70. The scores in Fabric-0.7 and 16 HL were significantly higher than those of Fabric-0.9 and 3 at days 35 and 70 (p<0.05).

2-2. immunohistochemical findings

The microscopic views and scores of α-SMA are shown in Figure 5. With Fabric-0.7, α-SMA positive cells were seen sparsely in the superficial layers of the fabric from day 7 (0.42 ± 0.49) and peaked at day 14 (0.50 ± 0.55) but were barely visible at day 35. With Fabric-0.9 and 3, small amounts of α-SMA positive cells were seen throughout all layers of the fabric at day 7 (0.33 ± 0.52 and 0.50 ± 0.55), but were barely visible at day 35. With Fabric-16, especially in the holes, a lot of α-SMA positive cells were seen throughout all layers of the fabric at day 7 (1.67 ± 0.52) and peaked at day 14 (2.00 ± 0.63). The cells then decreased gradually until day 70. The score in Fabric-16 HL was significantly higher than those in Fabric-0.7, 0.9, 3 and 16 FB at days 7 and 14 (p<0.05).

The microscopic views and scores of collagen type I are shown in Figure 6. Collagen type I in Fabric-0.7 was seen in the superficial layers of the fabrics and increased massively throughout all layers of the fabric until day 35 (1.83 ± 0.41) and hardly decreased at day 70 (2.17 ± 0.41). With Fabric-0.9 and 3, the collagen was seen throughout all layers of the fabric at day 7 (0.50 ± 0.55 and 0.33 ± 0.52) and increased mildly until day 35 (1.00 ± 0.00 and 0.83 ± 0.41) and was maintained until day 70 (1.00 ± 0.00 and 1.17 ± 0.41). With Fabric-16, the collagen was seen from day 3 (0.67 ± 0.52) in the hole and from day 7 (0.50 ± 0.55) around the bundles. Especially, in the hole, the collagen massively increased until day 35 (2.17 ± 0.41) and hardly decreased until day 70 (2.33 ± 0.52). The scores with Fabric-0.7 and 16 HL were significantly higher than those with Fabric-0.9, 3 and 16 FB at days 35 and 70 (p<0.05).

The microscopic views and scores of collagen type III are shown in Figure 7. Collagen type III in Fabric-0.7 was seen in the superficial layers of the fabrics and increased throughout all layers by day 7 (1.00 ± 0.00) and hardly decreased until day 70 (0.50 ± 0.55). In Fabric-0.9 and 3, the collagen was seen throughout all layers of the fabric at day 3 (0.33 ± 0.52 and 0.33 ± 0.52) and increased mildly at day 7 (1.33 ± 0.52 and 1.17 ± 0.41) and was maintained until day 70 (0.83 ± 0.41

and 0.67 ± 0.52). In Fabric-16, the collagen was seen at day 3 (0.33 ± 0.52 and 0.33 ± 0.52) both in the holes and around the bundles. Especially, in the hole, the collagen increased massively at day 7 (2.55 ± 0.42) and hardly decreased until day 70 (1.67 ± 0.52). The scores in the Fabric 16 HL were significantly higher than those in the Fabric-0.7, 0.9, 3 and 16 FB at days 7, 14 and 35 (p<0.05).

The microscopic views and scores of VWF are shown in Figure 8. VWF positive cells in Fabric-0.7 were seen in the superficial layers at day 7 (0.83 ± 0.41) and increased in number until day 14 (1.00 ± 0.00), being subsequently, maintained until day 70 (0.67 ± 0.52). With Fabric-0.9 and 3, slight infiltration of VWF positive cells was seen throughout all layers of the fabric at day 7 (0.50 ± 0.55 and 0.17 ± 0.41) and increased mildly until day 35 (1.17 ± 0.41 and 0.83 ± 0.41) and were maintained until day 70 (0.83 ± 0.41 and 0.83 ± 0.41). With Fabric-16, VWF positive cells were seen at day 7 (0.17 ± 0.41 and 0.33 ± 0.52) and increased gradually until day 70 (1.83 ± 0.41 and 1.33 ± 0.52) both around the bundles and in the holes. The score of VWF in Fabric-16 FB was significantly higher than those in Fabric-0.7, 0.9 and 3 (p<0.05).

The microscopic views and scores of CD68 are shown in Figure 9. A few CD68 positive cells stained for M1 macrophages in Fabric-0.7 were seen at day 3 (0.33 ± 0.52) in the superficial layers and increased rapidly by day 14 (1.67 ± 0.82), but decreased quickly by day 70 (0.33 ± 0.52). With Fabric-0.9 and 3, the cells were seen a few throughout all layers of the fabric at day 3 (1.00 ± 0.00 and 0.83 ± 0.75) and increased gradually and mildly until day 35 (1.17 ± 0.41 and 1.50 ± 0.55) and then disappeared mostly at day 70 (0.67 ± 0.52 and 0.33 ± 0.52). With Fabric-16, the cells were seen throughout all layers of the fabric, especially around the bundles at day 3 (1.00 ± 0.00) and increased massively at day 14 (2.00 ± 0.63) and hardly decreased until day 70 (2.00 ± 0.63). The score in Fabric-16 FB was significantly higher than those in Fabric-0.7, 0.9 and 3 at day 70 (p<0.05).

The microscopic views and scores of CD163 are shown in Figure 10. CD163 positive cells stained for M2 macropharges in Fabric-0.7 were sparsely seen at day 3 (1.17 ± 0.41) in the superficial layers and increased mildly at day 7 (2.00 ± 0.63) and decreased gradually until day 70 (0.83 ± 0.41). However, with Fabric-0.9 and 3, a lot of CD163 positive cells were seen at day 3 (1.83 ± 0.41 and 1.33 ± 0.52) and increased massively until day 14 (2.67 ± 0.52 and 2.67 ± 0.52) and

decreased gradually until day 70 (1.00 ± 0.00 and 1.00 ± 0.00). With Fabric-16, the cells were rarely seen at day 3 (0.67 ± 0.52). The cells increased gradually until day 14 (1.50 ± 0.55) and then decreased until day 70 (0.50 ± 0.55) both around the bundles and in the holes. The scores in the Fabric-0.9 and 3 were significantly higher than those in Fabric-16 FB and HL at day 7 and those in Fabric-0.7, 16 FB and HL at day 14 (p<0.05).

DISCUSSION

So far, several *in vitro* studies have reported the effect of fiber diameter and spacing-size on the cellular adhesion, proliferation and differentiation[5,6,8,10,16,17]. For instance, Saino et al. evaluated four different fiber diameters and alignments of PLLA scaffolds (0.1-1.6 μm) and showed pro-inflammatory cytokine secretion was more strongly affected by fiber diameter than by fiber alignment.[16] Jung et al. assessed the proliferation and infiltration of bone marrow stem cells into poly-lactic acid (PLLA) nanofibers, with pore sizes of 2 to 20 μm, *in vitro*[17]. They confirmed that the cells were unable to infiltrate into the nanofibers with a small pore size (2-6 μm), but were able to infiltrate into the nanofibers with a bigger pore size (10-20 μm). In the present study, we examined how fiber diameter and space-size of non-woven fabrics affect the cellular response and tissue remodeling, especially using an *in vivo* rat dorsal implantation model. To evaluate the effects of fiber diameter and spacing-size, we used four types of non-woven PGA fabrics with different fiber diameter and spacing-size; Fabric-0.7 (thin fiber diameter and narrow spacing-size), Fabric-0.9 (thin fiber diameter and medium spacing-size), Fabric-3 (middle fiber diameter and medium spacing-size) and Fabric-16 (thick fiber diameter and broad spacing-size) as shown in Table 3.

Initially, inflammatory cell infiltration, granulation tissue formation and connective tissue accumulation were observed and evaluated semi-quantitatively after H&E staining and Masson Trichrome staining. In Fabric-0.7 with thin fiber diameter and narrow spacing-size, the inflammatory cells accumulated mainly on the surface of the fabric initially. Then, the cells and granulation tissue gradually infiltrated all layers of the fabric, and finally, excessive connective tissue accumulated with the rapid degradation of the fabric, forming a dense scar. In Fabric-16 with thick fiber diameter and

broad spacing-size, the inflammatory responses were seen initially and continue with the massive accumulation of the cells and tissue until day 70 with continuous degradation of the fabric, especially around the bundle, finally, forming dense scar. In contrast, in Fabric-0.9 and 3 (thin and middle fiber diameter, and medium spacing-size), inflammatory cells and granulation tissue were obvious in all layers of the fabric initially, but the reaction then gradually decreased until day 70. Only mild formation of connective tissue was seen finally, creating more favorably remodeled tissue with less scar and adequate thickness of the tissue. Thus, too narrow or too broad fiber space was considered to induce dense scar formation, although the chronological courses differed depending on the degradation periods of the fabrics.

Next, to evaluate the mechanism underlying such scar formation, we investigated the existent of myofibroblast and the production of collagen by α-SMA or collagen type I and III stainning. In Fabric-0.7, myofibroblasts appeared and gathered intensively around the fabrics initially. Collagen levels then massively increased (initially type III and later type I), finally remodeling scar tissue. In contrast, in Fabric-0.9 and 3, only a few myofibroblasts were noted, and the formation of collagen type I and III was mild, with relatively little scar. Several previous reports described that the transition from fibroblasts to myofibroblasts depends on the structure of the scaffold[11,18,19]. Yannas et al. reported that in a porous collagen scaffold (20-120 μm), myofibroblasts comprised only about 10% of the total number of fibroblasts without wound contraction. In contrast, in the absence of a porous structure, myofibroblasts comprised 50% of the total number of fibroblasts with wound contraction[18]. As in their study, our results also showed that Fabric-0.9 and 3 with their appropriate fiber space induced a smaller composition of myofibroblasts and wound contraction than Fabric-0.7 or 16. In another previous report, fibroblasts were estimated to differentiate into myofibroblasts due to abnormal tissue remodeling with little three-dimensional extracellular matrix and acquisition of tractional forces[20]. Consequently, the presence of many myofibloblasts causes massive collagen accumulation and scar formation with tractional shrinks[21-23]. In the present study, Fabric-16, which has a relatively broad fiber space and little matrix, especially Fabric-16 HL, was estimated to induce pathological myofibroblasts differentiation and the excessive collagen type I and III accumulation,

finally resulting in remodeling with dense scar tissues.

In the wound repair process, changes in wound matrix composition follow a certain pattern over time. Type III collagen are generally beginning to be produced after injury. The initial type III collagen is replaced by type I collagen until a later phase of wound healing[24-27]. Particularly, in fibrotic scar, a marked increase in collagen type I was noted compared with other matrix components[26]. Thus, the narrow fiber space of Fabric-0.7 and broad fiber space of Fabric-16 appear to affect the myofibroblasts differentiation, inducing massive collagen production with rapid or continuous transition from type III to I, and ultimately resulting in remodeled tissue with scarring. In contrast, an adequate fiber space, such as that seen in Fabric-0.9 or 3 affects less myofibroblasts differentiation, moderate collagen production with mild transition from type III to I, and finally results in remodeled tissue with less scar.

Besides, we evaluated the vascular endothelial cell migration by staining with VWF to investigate the relationship between the fiber diameter or spacing-size of the artificial fabric and neovascularization. Jiang et al. previously evaluated five different types of three dimensional electrospun scaffolds of sodium tetrahydroborate in a rat dorsal implantation model for eight weeks. They found that a broad fiber space of the scaffold (≥20 μm) tended to induce more neovascularization, especially around the fiber[12]. In our study, in Fabric-0.7, with its relatively narrow fiber space, neovascularization was found almost only on the surface of the fabric early in the observation period and decreased until day 70. In Fabric-0.9 and 3, with their adequate fiber space, the number of vessels increased mildly throughout all layers of the fabric until day 35, and was maintained until day 70. However, in Fabric-16, with its broad fiber space, the number of vessels increased continuously, especially in the holes around the fiber bundles. Finally, at day 70, the number of vessels was much greater than in other fabrics. Thus, neovascularization may be associated with adequate fiber spacing. However, it may be also be affected by the difference of fiber degradation.

In previous reports, the inflammatory macrophage phenotype (M1), is characterized by CD68 cell surface markers in rats, promoting the production of large amounts of nitric oxide, other

reactive oxygen intermediates, copious amounts of pro-inflammatory cytokines (e.g. IL-12 and TNFα) and ultimately scar formation. Conversely, the anti-inflammatory macrophage phenotype (M2) is characterized by CD163 cell surface markers in rats, producing high levels of IL-10 and TGF-β expression or large amounts of arginase, inhibiting the release of pro-inflammatory cytokines or scavenge debris, promoting angiogenesis, and recruiting the cells involved in constructive tissue remodeling[29-34]. Therefore, we assessed the phenotype of the infiltrated macrophages (M1 or M2) in each fabric, as this phenotype might affect the final tissue remodeling. In our present study, with Fabric-0.7, many more inflammatory M1 macrophages than regenerative M2 macrophages were seen early around the surface of the fabric. However, rapid reductions in both M1 and M2 macrophages were seen later. In contrast, with Fabric-0.9 and 3, many regenerative M2 macrophages were observed early throughout all layer of the fabric, whereas M1 macrophages were considerably less frequent up to day 70. With Fabric-16, especially around the bundles (16 FB), many more M1 macrophages than M2 macrophages were seen early throughout all layers of the fabric, and their numbers remained high throughout the observation. Garg et al., reported that the mouse bone marrow-derived macrophages (BMMΦs) acquired a functional M2-like phenotype when in contact with a scaffold of pore size 14.73 μm, although BMMΦs showed an M1-like phenotype mainly on scaffolds with pore sizes 0.96 and 10.57 μm[7]. Thus, the too narrow and too broad fiber space with Fabric-0.7 or 16, respectively, caused a continuous inflammatory response with massive M1 macrophages, whereas the adequate fiber spacing with Fabric-0.9 and 3 induced less inflammatory tissue remodeling with plentiful presence of regenerative M2 macrophages.

Interestingly, although Fabric-0.7 and 0.9 have similar fiber diameters but different fiber spacing (approximately 2 and 19 μm), these fabrics showed different tissue reaction and remodeling. It may be likely due to the narrow or adequate fiber spaces compared with standard animal cell sizes (6-20 μm). In contrast, although Fabric-0.9 and 3 had different fiber diameters (nearly 3-fold different), but similar and adequate spacing-size (approximately 19 μm), these fabrics showed similar and favorable tissue reactions and remodeling to each other. These results indicated that the fiber spacing-size of the fabrics may be more important than their diameter for the tissue reaction and

remodeling. Garg et al. also reported in his *in vitro* experiment that the pore size of a scaffold is a more critical regulator of macrophage polarization compared to the fiber diameter.[7] Thus, if adequate fiber spacing with adequate fiber diameter is adopted to artificial scaffolds, more favorable tissue reaction and remodeling can be induced. Generally, the fiber diameter and fiber space of the natural extracellular matrix in the human body are approximately 0.01-2.0 μm and 10-20 μm, respectively[34,35]. Therefore, artificial scaffolds with such biomimic structures may realize more excellent tissue regeneration similar to natural tissue reaction[36].

CONCLUSION

The present study revealed that the non-woven fabrics with adequately adjusted spacing-size induced the infiltration of regenerative M2 macrophages and suppressed the infiltration of inflammatory M1 macrophages and myofibroblasts. Those fabrics were able to form moderate granulation tissue or connective tissues with a rapid transition from collagen type III to I, finally leading to excellent remodeled tissue with little scar formation and adequate tissue thickness. Therefore, optimizing the spacing-size as well as the fiber diameter of artificial scaffolds may control the cellar response and tissue remodeling and facilitate more favorable tissue regeneration without scar formation.

REFERENCES

1. Anna S.; Benjamin A. Using biomaterials to rewire the process of wound repair, Biomater Sci. **2017**, 5(8) 1421-1434 DOI: 10.1039/C7BM00295E

2. Geoffrey G.; Sabine W.; Yann B.; Michael TL. Wound repair and regeneration, Nature, **2008**, 453 314-321 DOI: 10.1038/nature07039

3. Reinke M.; Sorg H. Wound Repair and Regeneration, Eur Surg Res, **2012**, 49(1) 35-43 DOI: 10.1159/000339613

4. Mark H.; Katherine S.; Zoe W.; Rachel M. Macrophage Phenotypes Regulate Scar Formation and Chronic Wound Healing, Int. J. Mol. Sci., **2017**, 18(7) 1545 DOI: 10.3390/ijms18071545

5. Federica R.; Simone P.; Daniele P.; Federica P.; Marco G.; Francesco N.; Alessandra E.; Luigi V.; Mirella G.; Maria B. Regulation of human Macrophage M1–M2 Polarization Balance by hypoxia and the Triggering receptor expressed on Myeloid cells-1, Front. Immunol., **2017**, 8 1097 DOI: 10.3389/fimmu.2017.01097

6. Molly O.; Claire S.; Sraeyes S.; Edward B. Monocytes and macrophages in tissue repair: Implications for immunoregenerative biomaterial design, Experimental Biology and Medicine, **2016**, 241(10) 1084-1097 DOI: 10.1177/1535370216650293

7. Garg K.; Pullen A.; Oskeritzian A.; Ryan J.; Bowlin L. Macrophage functional polarization (M1/M2) in response to varying fiber and pore dimensions of electrospun scaffolds, Biomaterials, **2013**, 34(18) 4439-4451 DOI: 10.1016/j.biomaterials.2013.02.065

8. Bartneck M.; Schulte A.; Paul E.; Diez M.; Lensen C.; Zwadlo G. Induction of specific macrophage subtypes by defined micro-patterned structures. Acta Biomater. **2010**, 6(10) 3864–72 DOI: 10.1016/j.actbio.2010.04.025

9. Joern Z.; Alexander M.; Norbert S.; Bjoern S.; Martin D.; Hagen S. Chondrogenic differentiation of human articular chondrocytes differs in biodegradable PGA/PLA scaffolds. Tisuue Engineering, **2007**, 13(9) 2335-2343 DOI: 10.1089/ten.2006.0393

10. Mario A.; Julie L.; Grissel S.; Byung C.; Ajaykumar V.; Amir G.; Ali K. Delivery strategies to control inflammatory response: Modulating M1-M2 polarization in tissue engineering applications, J Control Release., **2016**, 240 349-363 DOI: 10.1016/j.jconrel.2016.01.026

11. Yannas V.; Lee E.; Orgill P.; Skrabut M.; Murphy F. Synthesis and characterization of a model extracellular matrix that induces partial regeneration of adult mammalian skin., Proc. Nati. Acad. Sci., **1989**, 86(3) 933-937 DOI: 10.1073/pnas.86.3.933

12. Jiang J.; Zhuoran L.; Hongjun W.; Yue W.; Mark C.; Matthew T.; Matthew E.; Linxia G.; Jingwei X. Expanded Three-dimensional Nanofiber Scaffolds: Cell Penetration, Neovascularization, and Host Response., Adv Healthc Mater., **2016**, 5(23) 2993-3003 DOI: 10.1002/adhm.201600808

13. Li J.; Laurencin T.; Caterson J.; Tuan S.; Ko K. Electrospun nanofibrous structure: a novel scaffold for tissue engineering, J Biomed Mater Res, **2002**, 60(4) 613-621 DOI: 10.1002/jbm.10167

14. Feng Z.; Rong G. Manufacturing technologies of polymeric nanofibers and nanofibers nanofubre yarns. Polymer International, **2008**, 57(6) 837-845 DOI: 10.1002/pi.2395

15. Jana H.; Marketa K.; Jakub E.; Andrea K.; Vit N.; Lubos B.; Jiri C. Impact of Various Sterilization and Disinfection Techniques on Electrospun Poly- ε -caprolactone. ACS Omega, **2020**, 5 8885-8892 DOI: 10.1021/acsomega.0c00503

16. Saino E.; Focarete L.; Gualandi C.; Emanuele E.; Cornaglia I.; Imbriani M. Effect of electrospun fiber diameter and alignment on macrophage activation and secretion of proinflammatory cytokines and chemokines. Biomacromolecules. **2011**, 12 1900–1911. DOI: 10.1021/bm200248h

17. Jung L.; Sung J.; Min B.; Dae Y.; Dong H.; Chun K.; Eben A.; Il K. Highly Porous Electrospun Nanofibers Enhanced by Ultrasonication for Improved Cellular Infiltration., Tissue Engineering A, **2011**, 17(21-22) 2695-2702 DOI: 10.1089/ten.TEA.2010.0709

18. Yannas V.; Emerging rules for inducing organ regeneration, Biomaterials **2013**, 34(2) 321-330 DOI: 10.1016/j.biomaterials.2012.10.006

19. Murphy F.; Orgill P.; Yannas V. Partial dermal regeneration is induced by biodegradable collagen glycosaminoglycan grafts, Lab Invest, **1990**, 62(3) 305-313

20. Hinz B.; Phan H.; Thannickal J.; Galli A.; Bochaton L.; Gabbiani G. The myofibroblast: one function, multiple origins, Am J Pathol, **2007**, 170(6) 1807-1816 DOI: 10.2353/ajpath.2007.070112

21. Hinz B. Formation and function of the myofibroblast during tissue repair, J Invest Dermatol, **2007**,127(3) 526–537 DOI: 10.1038/sj.jid.5700613

22. Hinz B. Masters and servants of the force: the role of matrix adhesions in myofibroblast force perception and transmission, Eur J Cell Biol, **2006**, 85(3-4) 175-181 DOI: 10.1016/j.ejcb.2005.09.004

23. Hinz B.; Mastrangelo D.; Iselin C.; Chaponnier C.; Gabbiani G. Mechanical tension controls granulation tissue contractile activity and myofibroblast differentiation, Am. J. Pathol, **2001**, 159(3) 1009–1020 DOI: 10.1016/S0002-9440(10)61776-2

24. Singer J.; Clark A. Cutaneous wound healing, N Engl J Med, **1999**, 341(10) 738-746 DOI: 10.1056/NEJM199909023411006

25. Witte B.; Barbul A. General principles of wound healing, Surg Clin North Am, **1997**, 77(3) 509-

528 DOI: 10.1016/s0039-6109(05)70566-1

26. Lovvorn N.; Cheung T.; Nimni E.; Perelman N.; Estes M.; Adzick S. Relative distribution and crosslinking of collagen distinguish fetal from adult sheep wound repair, J Pediatr Surg, **1999**, 34(1) 218-223 DOI: 10.1016/s0022-3468(99)90261-0

27. Betz P.; Nerlich A.; Wilske J.; Tübel J.; Penning R.; Eisenmenger W. Analysis of the immunohistochemical localization of collagen type III and V for the time-estimation of human skin wounds, Int J Legal Med, **1993**, 105(6) 329-332 DOI: 10.1007/BF01222117

28. Leask A. The role of endothelin-1 signaling in the fibrosis observed in systemic sclerosis, Pharmacol Res, **2011**, 63(6) 502-503 DOI: 10.1016/j.phrs.2011.01.011

29. Gordon S.; Taylor R. Monocyte and macrophage heterogeneity, Nat. Rev. Immunol., **2005**, 5 953-964 DOI: 10.1038/nri1733

30. Mantovani A.; Sica A.; Locati M. Macrophage polarization comes of age., Immunity, **2005**, 23(4) 344-346 DOI: 10.1016/j.immuni.2005.10.001

31. Mosser M. The many faces of macrophage activation, J Leukocyte Biol., 2003, 73(2) 209-212 DOI: 10.1189/jlb.0602325

32. Badylak F.; Gilbert W. Immune response to biologic scaffold materials., Semin Immunol., **2008**, 20(2) 109-116 DOI: 10.1016/j.smim.2007.11.003

33. Madden R.; Mortisen J.; Sussman M.; Dupras K.; Fugate A.; Cuy L.; Hauch D.; Laflamme A.; Murry E.; Ratner D. Proangiogenic scaffolds as functional templates for cardiac tissue engineering., Proc Natl Acad Sci., **2010**, 107(34) 15211-15216 DOI: 10.1073/pnas.1006442107

34. Willis L.; Sabeh F.; Li Y.; Weiss J. Extracellular matrix determinants and the regulation of cancer cell invasion stratagems., J Microsc., **2013**, 251(3) 250–260 DOI: 0.1111/jmi.12064

35. Renaud P.; Olivier C.; Floria L.; Maryse R.; Marcel D.; Matthieu P.; Philippe C. Contractility of the cell rear drives invasion of breast tumor cells in 3D Matrigel, PNAS., **2011**, 108(5) 1943-1948 DOI: 10.1073/pnas.1010396108

36. Frederick S.; Joseph F.; Gurinder S. Collagen self-assembly and the development of tendon mechanical properties, Journal of Biomechanics, **2003**, 36(10) 1529-1553 DOI: 10.1016/S0021-

9290(03)00135-0

Figure Captions

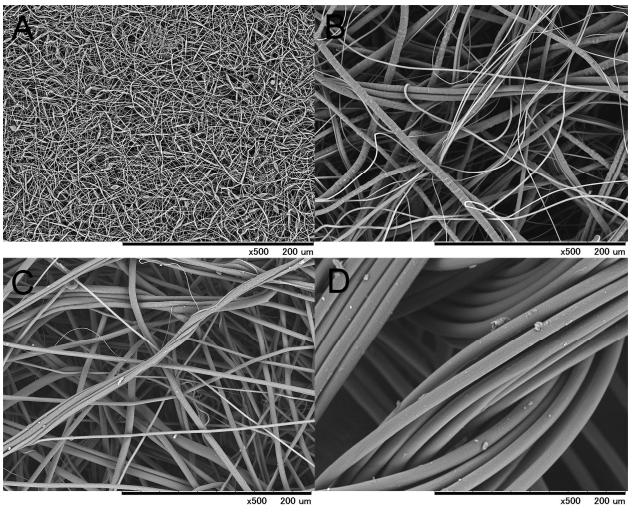

FIGURE 1. SEM micrographs demonstrating the architecture of the top layer (A: Fabric-0.7, B: Fabric-0.9, C: Fabric-3 D: Fabric-16). (×500) The fiber in Fabric-0.7 is denser than that in Fabric-0.9 and 3. Fabric-16 has a structure composed of two kinds of locations with different spacing-sizes: the "fiber bundle" and the "hole".

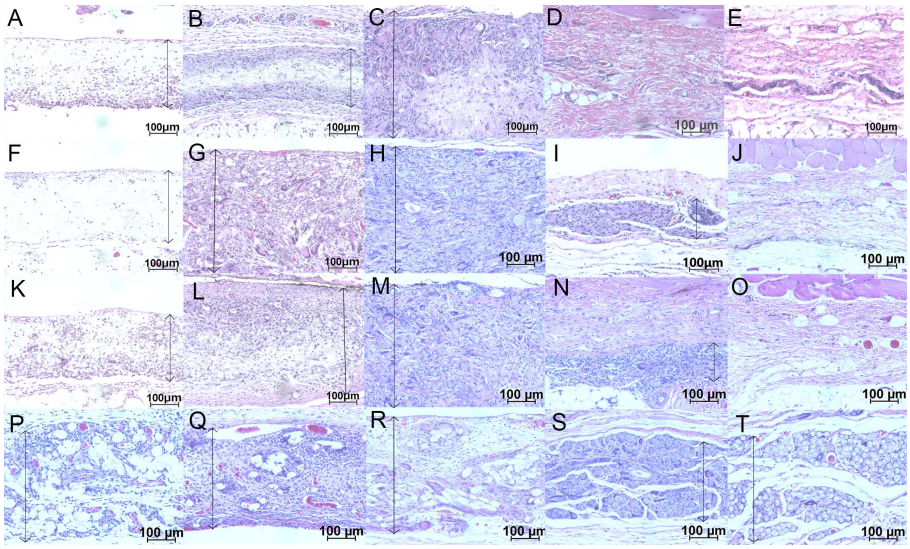

FIGURE 2. Images of hematoxylin-eosin staining at postoperative days 3, 7, 14, 35 and 70. (×200) ↕: layer of PGA nonwoven fabrics and remodeling tissue. (A-E: Fabric-0.7, F-J: Fabric-0.9, K-O: Fabric-3, P-T: Fabric-16).

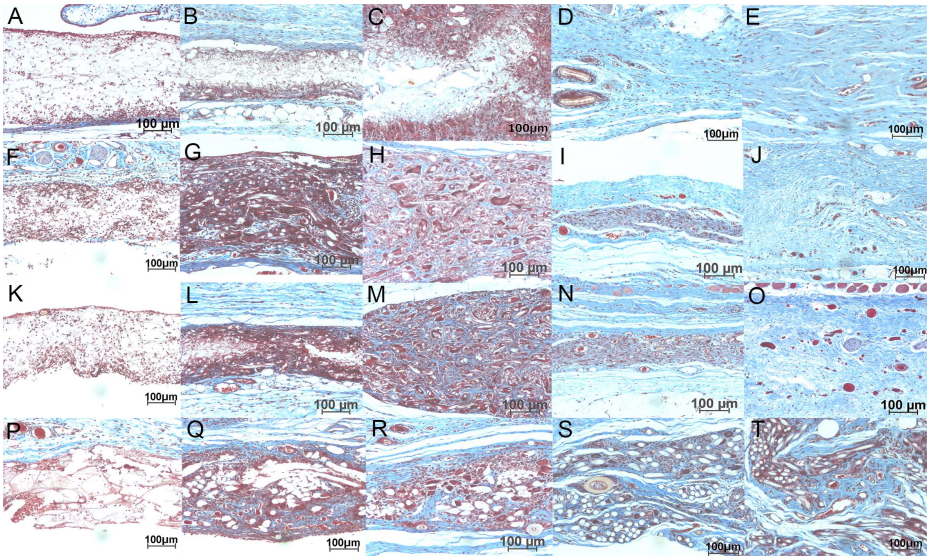

FIGURE 3. Images of Masson trichrome staining at postoperative days 3, 7, 14, 35 and 70 (×200) (A-E: Fabric-0.7, F-J: Fabric-0.9, K-O: Fabric-3, P-T: Fabric-16).

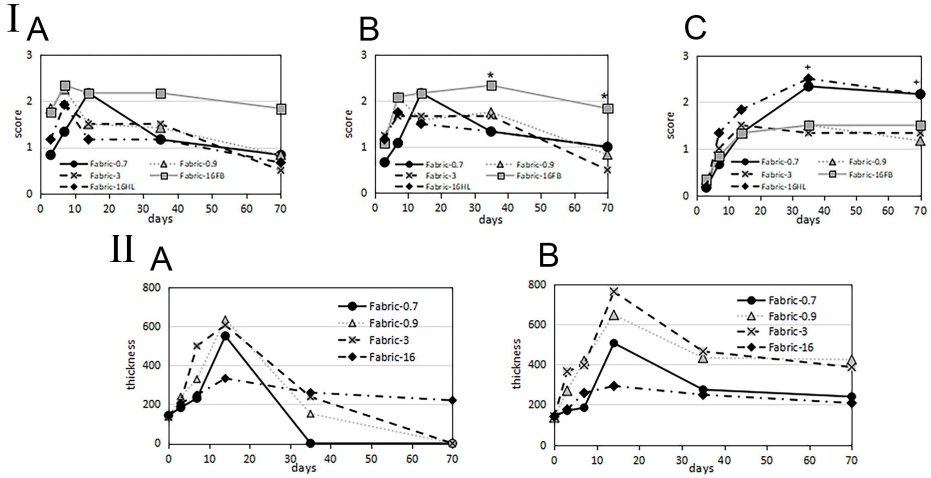

FIGURE 4. I. The histological scores of each fabric in hematoxylin-eosin staining and Masson trichrome staining. (A:inflammatory cells B: granulation tissue C:connective tissue) *: The scores of inflammatory cells and granulation tissue in Fabric-16 FB were significantly higher than those of Fabric-0.7 and 16 HL at day 35 and those of Fabric-0.7, 0.9, 3 and 16 HL at day 70 ($p<0.05$). +: The scores of connective tissue in Fabric-0.7 and 16 HL were significantly higher than those of Fabric-0.9 and 3 at day 35 and 70 ($p<0.05$). II. A: The thickness of each fabric. B: The thickness of the tissue induced by each fabric.

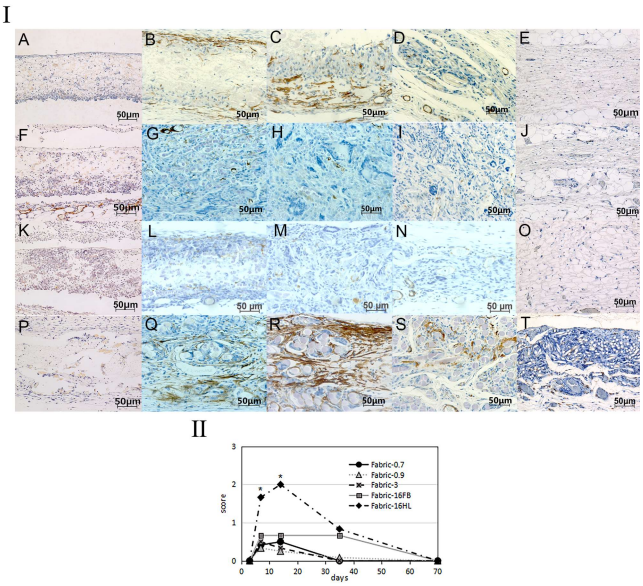

FIGURE 5. I. Images of immunohistochemical staining for α-SMA at postoperative days 3, 7, 14, 35 and 70 (×400) (A-E: Fabric-0.7, F-J: Fabric-0.9, K-O: Fabric-3, P-T: Fabric-16). II. The histological scores of each fabric for α-SMA. *: The score in Fabric-16 HL was significantly higher than those in Fabric-0.7, 0.9, 3 and 16 FB at days 7 and 14 ($p<0.05$).

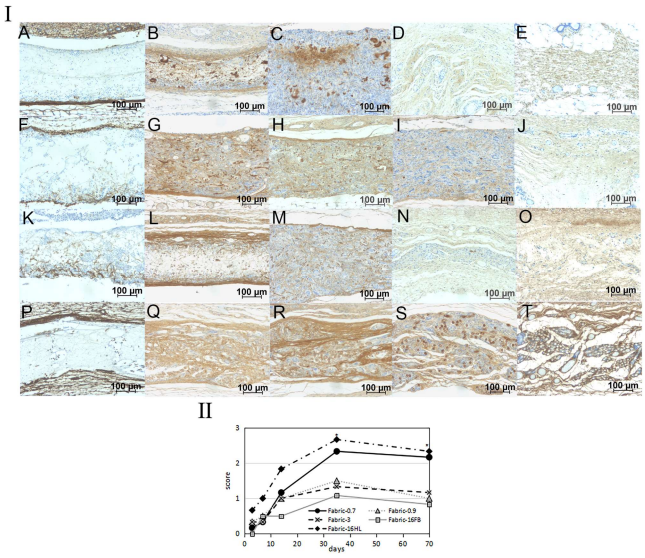

FIGURE 6. I. Images of immunohistochemical staining for type I collagen at postoperative days 3, 7, 14, 35 and 70 (×200) (A-E: Fabric-0.7, F-J: Fabric-0.9, K-O: Fabric-3, P-T: Fabric-16). II. The histological scores of each fabric for type I collagen. *: The scores in Fabric-0.7 and 16 HL were significantly higher than those in the Fabric-0.9, 3 and 16 FB at days 35 and 70 ($p<0.05$).

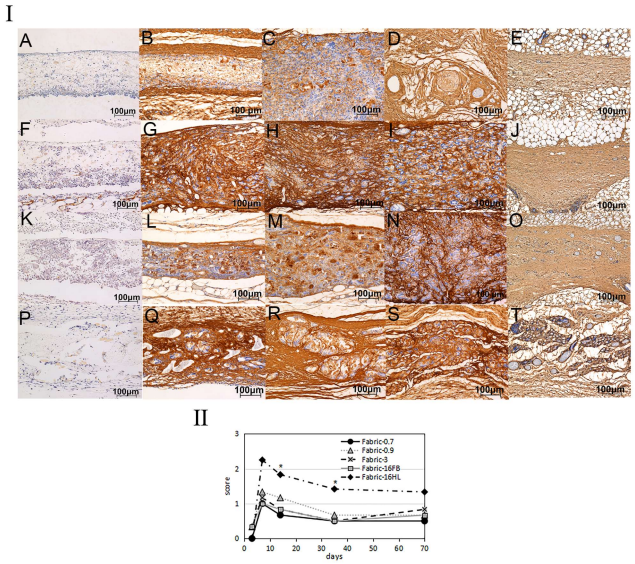

FIGURE 7. I. Images of immunohistochemical staining for type III collagen at postoperative days 3, 7, 14, 35 and 70 (×200) (A-E: Fabric-0.7, F-J: Fabric-0.9, K-O: Fabric-3, P-T: Fabric-16). II. The histological scores of each fabric for type III collagen. *: The score in the Fabric 16 HL was significantly higher than those in Fabric-0.7, 0.9, 3 and 16 FB at days 7, 14 and 35 ($p<0.05$).

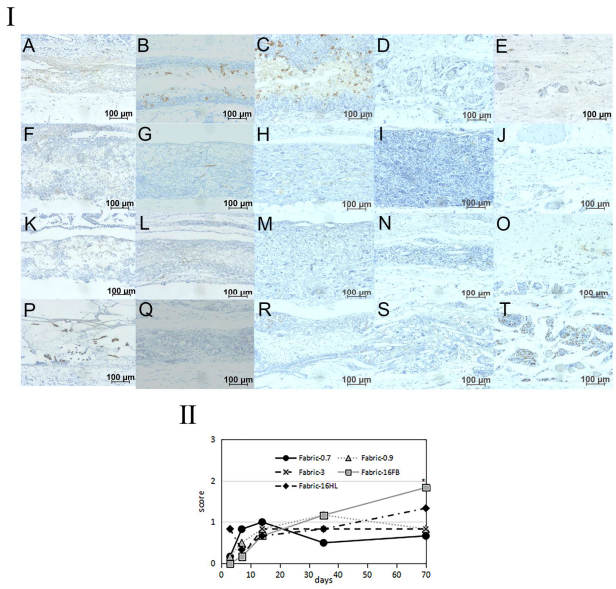

FIGURE 8. I. Images of immunohistochemical staining for VWF at postoperative days 3, 7, 14, 35 and 70 (×200) (A-E: Fabric-0.7, F-J: Fabric-0.9, K-O: Fabric-3, P-T: Fabric-16). II. The histological scores of each fabric for VWF. *: The score of VWF in Fabric-16 FB was significantly higher than those in Fabric-0.7, 0.9 and 3 ($p<0.05$).

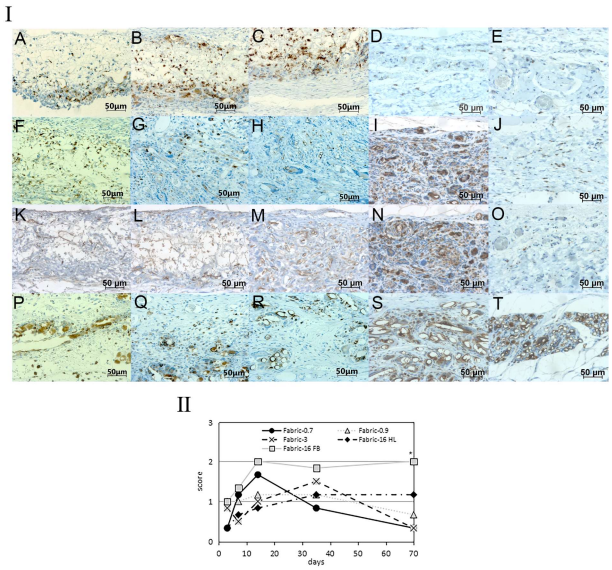

FIGURE 9. I. Images of immunohistochemical staining for CD68 at postoperative days 3, 7, 14, 35 and 70 (×400) (A-E: Fabric-0.7, F-J: Fabric-0.9, K-O: Fabric-3, P-T: Fabric-16). II. The histological scores of each fabric for CD68. *: The score in Fabric-16 FB was significantly higher than those in Fabric-0.7, 0.9 and 3 at day 70 ($p<0.05$).

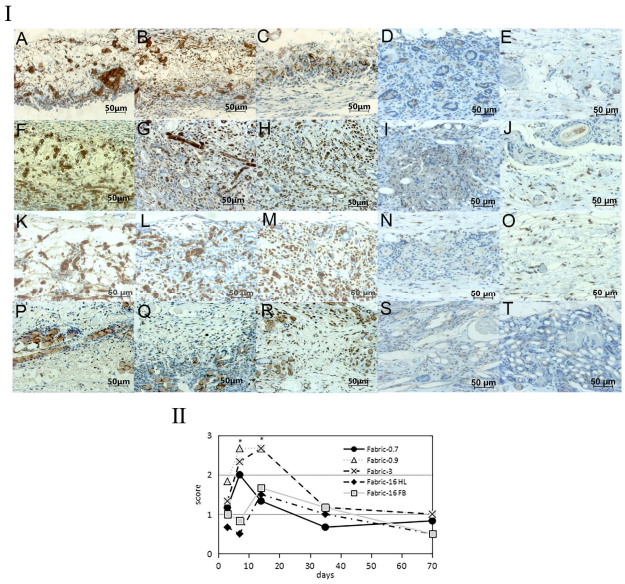

FIGURE 10. I. Images of immunohistochemical staining for CD163 at postoperative days 3, 7, 14, 35 and 70 (×400) (A-E: Fabric-0.7, F-J: Fabric-0.9, K-O: Fabric-3, P-T: Fabric-16). II. The histological scores of each fabric for CD163. *: The scores in Fabric-0.9 and 3 were significantly higher than those in Fabric-16 FB and HL at day 7 and those in Fabric-0.7, 16 FB and HL at day 14 ($p<0.05$).

Table of Contents

TABLE I. The histological scores for inflammatory cells, granulation tissue, and connective tissue

Category and Description	Score
(Inflammatory cells)	
No infiltration of inflammatory cells such as neutrophils, lymphocytes, and monocytes	0
Sparse infiltration of inflammatory cells	1
Focal infiltration of inflammatory cells	2
Diffuse infiltration of inflammatory cells	3
(Granulation tissue)	
No granulation tissue formation	0
Sparse or focal granulation tissue formation	1
Thin layer of granulation tissue	2
Thick layer of granulation tissue	3
(Connective tissue)	
No fibrous connective tissue formation	0
Sparse or focal connective tissue formation	1
Thin layer of fibrous connective tissue	2
Thick layer of fibrous connective tissue	3

TABLE II. The histological scores for the presence of myofibroblasts, intensity of type I and III collagen, presence of migrated vessels and presence of M1 and M2 macrophages (CD86 and CD163)

Category and Description	Score
(myofibroblasts)	
no presence of myofibroblast	0
sparse infiltration of myofibroblasts	1
focal infiltration of myofibroblasts	2
diffuse infiltration of myofibroblasts	3
(Type I and III collagen)	
no specific intense of collagen	0
slightly intense of collagen	1
moderately intense of collagen	2
strongly intense of collagen	3
(vessels)	
no presence of vessel	0
sparse infiltration of vessels	1
focal infiltration of vessels	2
diffuse infiltration of vessels	3
(M1 or M2 macrophages)	
no presence of macrophage	0
sparse infiltration of macrophages	1
focal infiltration of macrophages	2
diffuse infiltration of macrophages	3

TABLE III. Fiber diameter and spacing-size of poly-glycolic acid nonwoven fabrics

	Fiber diameter (μm)	Spacing-size (μm)
Fabric-0.7	0.69 ± 0.28	2.0 ± 0.8
Fabric-0.9	0.90 ± 0.65	19.3 ± 7.8
Fabric-3	3.0 ± 1.86	19.0 ± 10.0
Fabric-16 FB	16.2 ± 1.10	5.0 ± 4.0
Fabric-16 HL		825.4 ± 126.9

Table of Contents Graphic